

## Supporting Informations

### **General and Selective Reductive Amination of Carbonyl Compounds Using a Core-Shell Structured $\text{Co}_3\text{O}_4/\text{NGr}@C$ Catalyst**

Tobias Stemmler, Felix A. Westerhaus, Annette-E. Surkus, Marga-M. Pohl, Kathrin Junge, Matthias Beller\*

Leibniz-Institut für Katalyse e.V. an der Universität Rostock, Albert-Einstein Str. 29a, Rostock, 18059, Germany

\*Corresponding author: [matthias.beller@catalysis.de](mailto:matthias.beller@catalysis.de)

#### **Table of contents:**

S1	Materials and methods
S2	STA measurement
S3	XPS measurement
S4	EPR measurement
S5	XRD measurement
S6	BET- and BJH-measurement
S7	General procedure for hydrogenation with different catalyst loading
S8	Catalyst recycling experiment
S9	References

## **S1. Materials and methods**

Nitro compounds, aldehydes, ketones, solvents, metal precursor  $\text{Co}(\text{OAc})_2$ , 1,10-Phenanthroline and other chemicals were obtained from various chemical companies. Carbon powder, VULCAN® XC72R with Code XVC72R and CAS No. 1333-86-4 was obtained from Cabot Corporation Prod. The pyrolysis experiments were carried out in Dekema-Austramat 624 oven.

TEM (Transmission Electron Microscopy) measurements were performed at 200 kV with an aberration-corrected JEM-ARM200F (JEOL, Corrector: CEOS). The microscope is equipped with a JED-2300 (JEOL) energy-dispersive x-ray-spectrometer (EDXS) for chemical analysis. The samples were deposited without any pretreatment on a holey carbon supported Cu-grid (mesh 300) and transferred to the microscope. The High-Angle Annular Dark Field (HAADF) and Annular Bright Field (ABF) images were recorded with a spot size of approximately 0.1nm, a probe current of 120 pA and a convergence angle of 30-36°. The collection semi-angles for HAADF and ABF were 70-170 mrad and 11-22 mrad, respectively.

XPS (X-ray Photoelectron Spectroscopy) data was obtained with a VG ESCALAB220iXL (ThermoScientific) with monochromatic Al  $K\alpha$  (1486.6 eV) radiation. The electron binding energies  $E_B$  were obtained without charge compensation. For quantitative analysis the peaks were deconvoluted with Gaussian-Lorentzian curves, the peak area was divided by a sensitivity factor obtained from the element specific Scofield factor and the transmission function of the spectrometer.

EPR spectra were recorded in X-band at 80 K and 290 K on a Bruker EMX CW-micro spectrometer equipped with an ER 4119HS-WI high-sensitivity cavity and a variable temperature control unit (microwave power: 6.64 mW, modulation frequency: 100 kHz, modulation amplitude: 1 G).

XRD powder patterns were recorded on a Stoe STADI P diffractometer, equipped with a linear Position Sensitive Detector (PSD) using Cu  $K\alpha$  radiation ( $\lambda = 1.5406 \text{ \AA}$ ). Processing and assignment of the powder patterns was done using the software WinXpov (Stoe) and the Powder Diffraction File (PDF) database of the International Centre of Diffraction Data (ICDD).

STA (Simultaneous Thermal Analysis) was performed with an NETZSCH STA 449 F3 *Jupiter*® for determining caloric effects and mass changes at the same time. The thermal scanning mode ranges from 30°C and 1100°C at a programming heating rate of 25 K/min. The gas flow is generally controlled by frits which are installed in the three gas flow channels with the following parameters: protective gas nitrogen (20 mL/min), purge gases nitrogen (60 mL/min) and air (80:20) (70 mL/min).

## S2. STA measurement

The dynamic TG (Thermogravimetry) and the corresponding DTG (Differential Thermogravimetry) and DSC (Differential Scanning Calorimetry) curves during the heat treatment of the immobilized Cobalt-phenanthroline-complex on carbon are illustrated in Figure 1. The DTG indicates a multi-stage pyrolysis. At least two features can be distinguished on the DTG curve. One feature appeared as a peak at around 100°C related to water desorption, if the material is not sufficiently dry. The most important feature is pointed out as a peak in a range of 200 to 400°C. The highest mass change takes place on the TGA trace and can be attributed to the sublimation of the excess of phenanthroline as well as the decomposition of the remained acetate ligand. GC-MS of the gas phase identified the formed sideproducts as CO, CO<sub>2</sub>, acetone and acetic acid except for the phenanthroline fragments. Furthermore, it is described in literature that the formation of CoO, Co<sub>3</sub>O<sub>4</sub> and metallic cobalt occur.[45],[46] Additionally, the endothermic DSC peak at 286 °C is due to the decomposition and solid-solid transition. While the TG and DTG traces up to 800°C show no significant changes of the sample, the DSC trace ended up with an endothermic process. It can be addressed to the formation of the *N*-doped graphene layers by carbonization of the remained phenanthroline ligand.

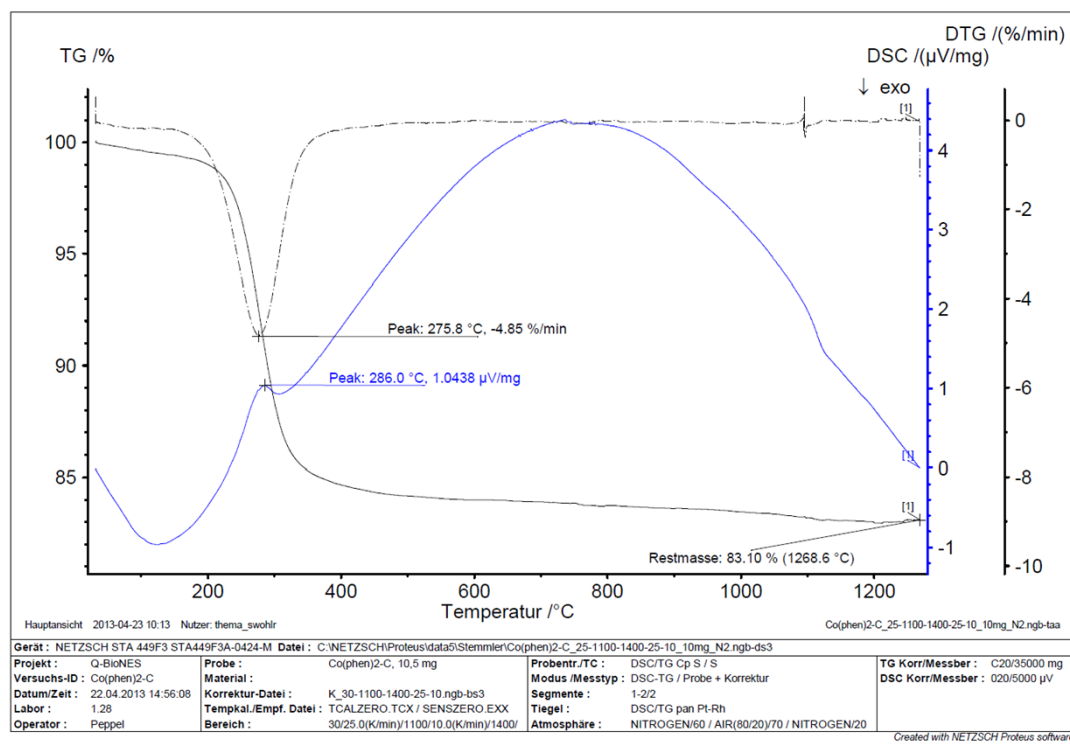


**Fig. S1. Simultaneous Thermal Analysis of the immobilized Cobalt-phenanthroline-complex on Vulcan carbon powder.**

## S3. XPS measurement

To obtain further insight into the structure of the catalyst surface and especially into the role of nitrogen coming from the organic ligand, XPS investigations of N and Co species were carried out. Interestingly, three distinct peaks are observed in the N1s spectra of the  $\text{Co}_3\text{O}_4@\text{C-N}_x$  catalyst with an electron binding energy of 399.0 eV, 400.8 eV and 402.3 eV (Fig. S2). The lowest binding energy peak can be attributed to pyridine-type nitrogen, which is bound to a metal ion.[47] The electron binding energy of 400.8 eV is characteristic for pyrrole-type nitrogen contributing two electrons to the carbon matrix. It is bound to a hydrogen atom. Such types of nitrogen are found after the carbonization of nitrogen-containing organic materials.[48] Finally, the small peak at 402.3 eV is typical for ammonium species like  $\text{NH}_4^+$  or  $\text{R-NH}_3^+$ .[49] The ratio between all Co atoms and all N atoms in the near surface region is 1:4.7. Deconvolution reveals that around 64% of all N atoms are bound to the metal ions. In the cobalt region, only peaks characteristic for oxidic Co are found (Fig. S3) with the typical binding energy of 780.4 eV of the  $\text{Co}2p_{3/2}$  and 795.3 eV of the  $\text{Co}2p_{1/2}$  electrons. Additionally, the satellite peaks at 786.7 eV and 802.8 eV are characteristic for oxidic Co. This agrees very well with TEM results, which suggest that the very small particles of 2-10 nm are oxidic and the bigger particles contain a Co core and a cobalt oxide shell. It is discussed in literature, that CoO on the surface is not stable and therefore oxidized to  $\text{Co}_3\text{O}_4$ .[50] Thus, it can be concluded that the surface of all Co-containing particles in the catalyst consists of  $\text{Co}_3\text{O}_4$ .

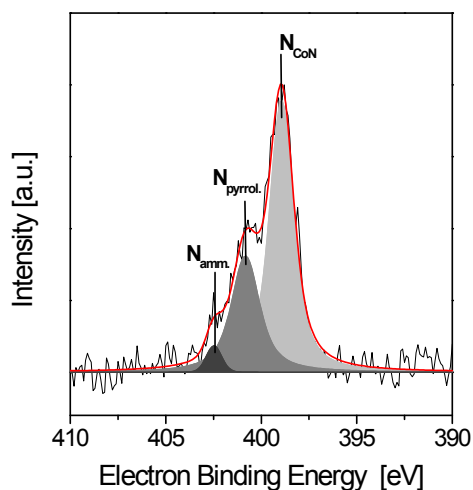


**Fig. S2.** N1s spectrum of the  $\text{Co}_3\text{O}_4/\text{NGr}@\text{C}$  catalyst. (different N1s state are:  $\text{N}_{\text{CoN}}$  N bound to Co;  $\text{N}_{\text{pyrrol.}}$ : pyrrolic N;  $\text{N}_{\text{amm.}}$ : N of ammonium species)

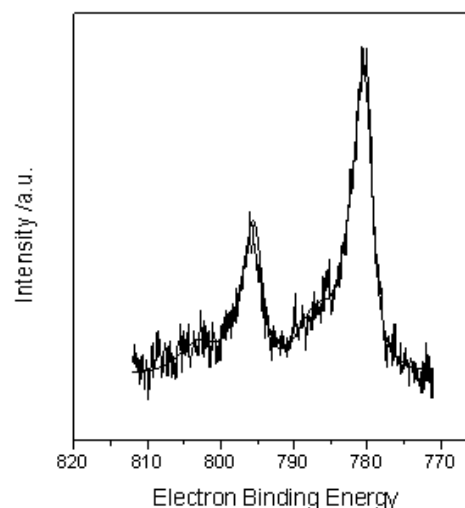


**Fig. S3.** Co2p spectrum of the catalyst with the typical features of  $\text{Co}_3\text{O}_4$ .

#### S4. EPR measurement

Besides TEM and EPR spectroscopy is another suitable method to gain information on the nature of Cobalt oxide containing particles. The EPR spectrum of the material contains a broad signal at  $g = 2.12$  (Fig. S4). The intensity of this signal increases slightly with rising temperature, which is characteristic for antiferromagnetic  $\text{Co}_3\text{O}_4$  particles. The Neel temperature  $T_N$  above which bulk  $\text{Co}_3\text{O}_4$  becomes paramagnetic is below 40 K [51, 52]. Previously it was found that the temperature dependence of the EPR signal intensity reflects very sensitively the onset of anti-ferromagnetic ordering in  $\text{Co}_3\text{O}_4$  and also in other antiferromagnetic oxide materials already well above  $T_N$  [53]. In bulk  $\text{Co}_3\text{O}_4$  the EPR intensity increased gradually up to 150 K and then remained constant up to 250 K before it started decreasing [52]. The observed intensity behaviour in Figure S6 is exactly in line with these previous results. The EPR signal at  $g = 2.12$  is superimposed on a second very broad anisotropic signal, the positive lobe of which is cut off at  $B = 0$ . This suggests that the magnetic properties are not exactly the same for each particle. The reason may be different particle sizes and/or replacement of O by N in the coordination of Co (as observed by XPS). In contrast to  $\text{Co}_3\text{O}_4$ , CoO is not expected to contribute to the EPR spectrum since CoO is antiferromagnetic below  $T_N \approx 293\text{K}$  [54] and thus EPR silent. Metallic Co is ferromagnetic up to a Curie temperature of  $1120^\circ\text{C}$  [55] and could in principle cause a ferromagnetic resonance signal, the intensity of which does not depend on temperature between 88 and 290 K.

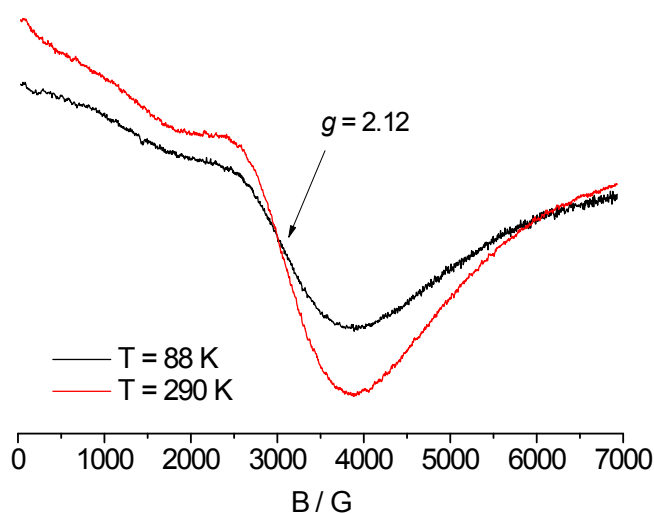


**Fig. S4.** EPR spectra of the  $\text{Co}_3\text{O}_4/\text{NGr}@C$  catalyst recorded at 88 and 290 K.

## **S5. XRD measurement**

The powder patterns of the catalyst Co-Co<sub>3</sub>O<sub>4</sub>/NGr@C for 1g-, 5g- and 10g-scale after pyrolysis are virtually identical, showing three characteristic peaks of metallic Co at 2 $\Theta$  = 44.16°, 51.42° and 75.84°. Additionally, the presence of Co<sub>3</sub>O<sub>4</sub> is confirmed by weak reflections at 2 $\Theta$  = 36.89°, 42.47° and 61.52°.

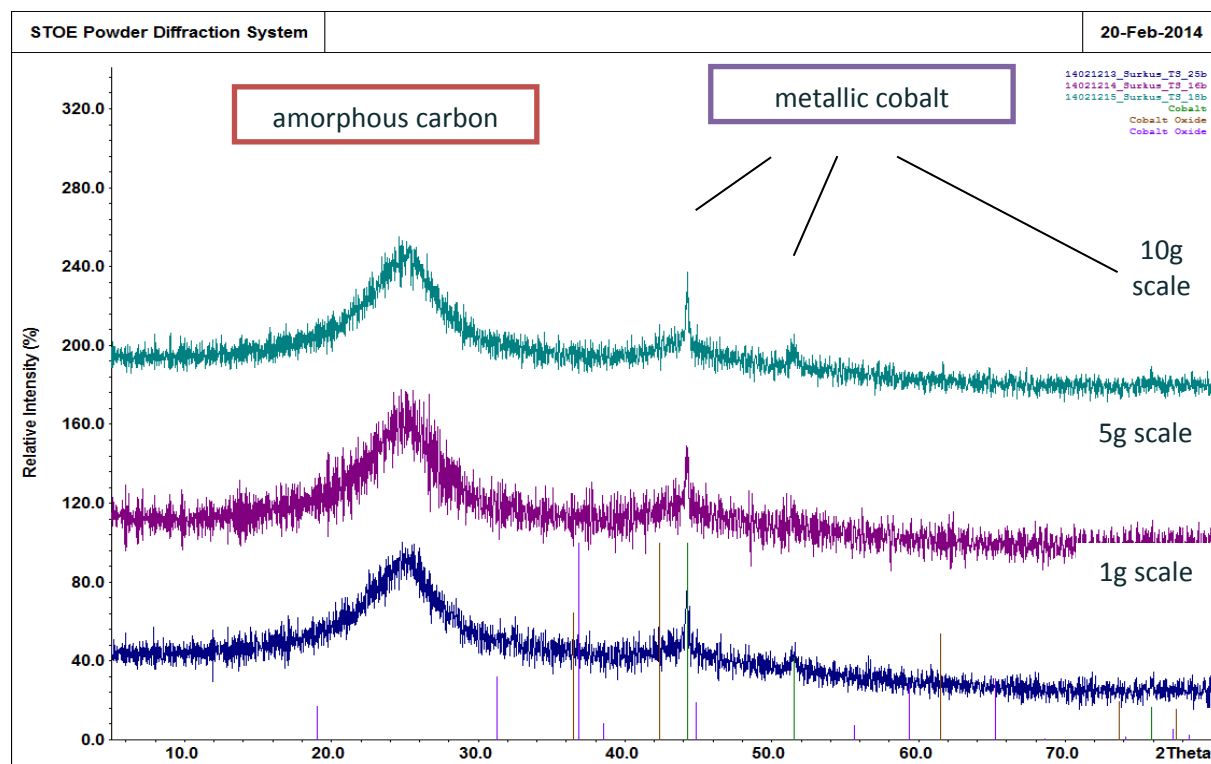


Fig. S5. Diffraction pattern of the Co<sub>3</sub>O<sub>4</sub>/NGr@C catalyst.

## S6. BET- and BJH-measurement

BET analysis provides precise specific surface area evaluation of materials by nitrogen multilayer adsorption measured as a function of relative pressure using a fully automated analyser. The BET surface area of  $\text{Co}_3\text{O}_4/\text{NGr}@C$  is  $102.1 \text{ m}^2/\text{g}$  and the corresponding average pore size is  $7.9 \text{ nm}$ , respectively (Fig. S8). It is about a mesoporous system and compare to the support Vulcan XC72R carbon powder itself (Fig. S9), the generated nanoparticles seal partially the present pores. Therefore, we observed a reduced surface area and pore volume combined with an increased average pore diameter. Figure S.6 shows pore diameter distribution by BJH, as obtained from the desorption part of the isotherms.

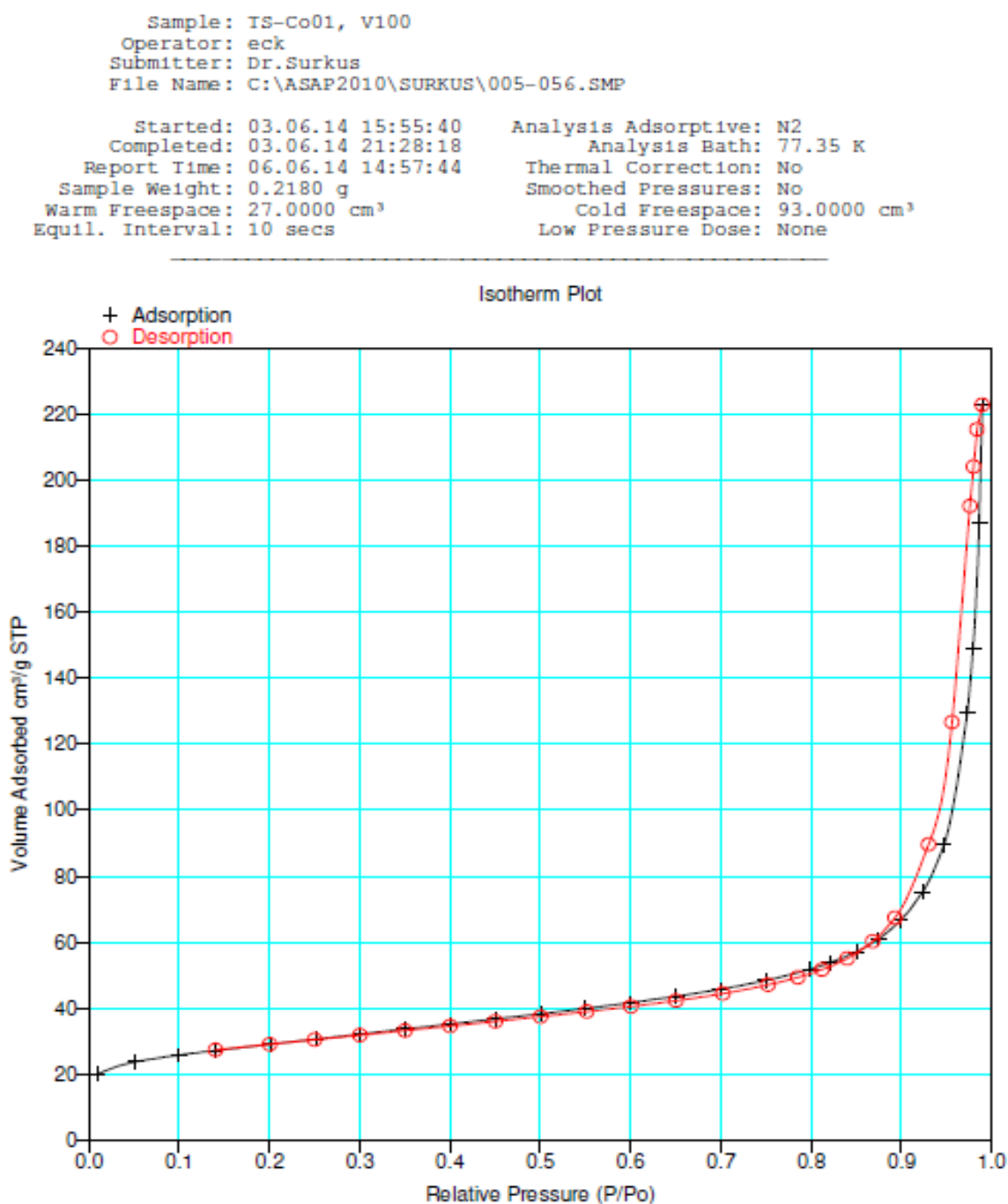


Fig. S6. Sorption isotherm of  $\text{Co}_3\text{O}_4/\text{NGr}@C$  catalyst.

Sample: IS-Co01, V100  
Operator: eck  
Submitter: Dr.Surkus  
File Name: C:\ASAP2010\SURKUS\005-056.SMP

Started: 03.06.14 15:55:40      Analysis Adsorptive: N2  
Completed: 03.06.14 21:28:18      Analysis Bath: 77.35 K  
Report Time: 06.06.14 14:57:44      Thermal Correction: No  
Sample Weight: 0.2180 g      Smoothed Pressures: No  
Warm Freespace: 27.0000 cm<sup>3</sup>      Cold Freespace: 93.0000 cm<sup>3</sup>  
Equil. Interval: 10 secs      Low Pressure Dose: None

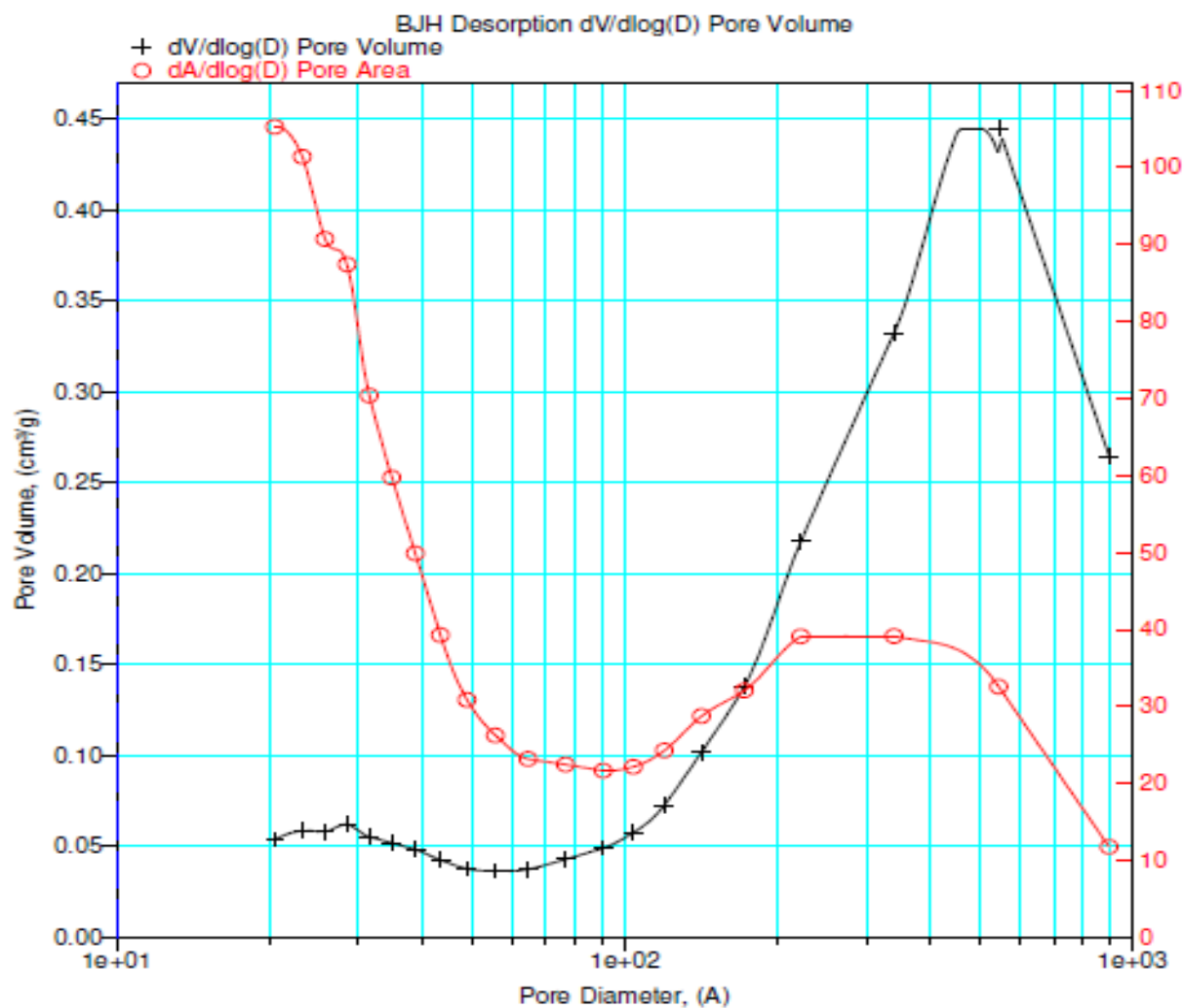


Fig. S7. Pore-size distribution calculated from the desorption isotherm for Co<sub>3</sub>O<sub>4</sub>/NGr@C catalyst.

Sample: TS-Co01, V100  
 Operator: eck  
 Submitter: Dr.Surkus  
 File Name: C:\ASAP2010\SURKUS\005-056.SMP  
  
 Started: 03.06.14 15:55:40      Analysis Adsorptive: N2  
 Completed: 03.06.14 21:28:18      Analysis Bath: 77.35 K  
 Report Time: 06.06.14 14:57:44      Thermal Correction: No  
 Sample Weight: 0.2180 g      Smoothed Pressures: No  
 Warm Freespace: 27.0000 cm<sup>3</sup>      Cold Freespace: 93.0000 cm<sup>3</sup>  
 Equil. Interval: 10 secs      Low Pressure Dose: None

-----  
 Summary Report

Area

Single Point Surface Area at P/Po 0.20085200 :	101.1882	m <sup>2</sup> /g
BET Surface Area:	102.0999	m <sup>2</sup> /g
BJH Desorption Cumulative Surface Area of pores between 10.000000 and 1000.000000 A Diameter:	68.8508	m <sup>2</sup> /g

Volume

Single Point Total Pore Volume of pores less than 741.9173 A Diameter at P/Po 0.97320344:	0.200340	cm <sup>3</sup> /g
BJH Desorption Cumulative Pore Volume of pores between 10.000000 and 1000.000000 A Diameter:	0.301787	cm <sup>3</sup> /g

Pore Size

Average Pore Diameter (4V/A by BET):	78.4880	A
BJH Desorption Average Pore Diameter (4V/A):	175.3278	A

**Fig. S8. Summary of the results of BET- and BJH-measurement of Co<sub>3</sub>O<sub>4</sub>/NGr@C catalyst.**

Sample: TS-CC01, V100  
 Operator: eck  
 Submitter: Dr.Surkus  
 File Name: C:\ASAP2010\SURKUS\005-057.SMP  
  
 Started: 04.06.14 12:03:03      Analysis Adsorptive: N2  
 Completed: 04.06.14 18:21:54      Analysis Bath: 77.35 K  
 Report Time: 06.06.14 14:58:13      Thermal Correction: No  
 Sample Weight: 0.2190 g      Smoothed Pressures: No  
 Warm Freespace: 27.0000 cm<sup>3</sup>      Cold Freespace: 93.0000 cm<sup>3</sup>  
 Equil. Interval: 10 secs      Low Pressure Dose: None  
 Analysis Conditions Modified During Analysis

-----  
 Summary Report

Area

Single Point Surface Area at P/Po 0.20214207 :	226.1393	m <sup>2</sup> /g
BET Surface Area:	226.2956	m <sup>2</sup> /g
BJH Desorption Cumulative Surface Area of pores between 10.000000 and 1000.000000 A Diameter:	56.8302	m <sup>2</sup> /g

Volume

Single Point Total Pore Volume of pores less than 729.4854 A Diameter at P/Po 0.97273592:	0.304945	cm <sup>3</sup> /g
BJH Desorption Cumulative Pore Volume of pores between 10.000000 and 1000.000000 A Diameter:	0.319163	cm <sup>3</sup> /g

Pore Size

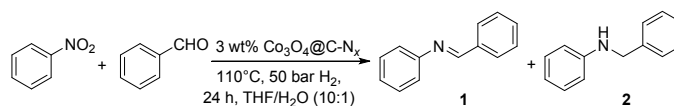
Average Pore Diameter (4V/A by BET):	53.9021	A
BJH Desorption Average Pore Diameter (4V/A):	224.6430	A

**Fig. S9. Summary of the results of BET- and BJH-measurement of Vulcan XC72R carbon powder.**

## **S7. General procedure for hydrogenation with different catalyst loading**

The following general procedure was used for the reductive amination of nitrobenzene with benzaldehyde. Into a reaction vial fitted with a magnetic stirring bar and a septum cap was added the cobalt-catalyst (2 mol%, 3wt% [Co] on carbon, 20 mg) followed by the nitrobenzene (0.5 mmol), benzaldehyde (1.0 mmol) and the solvent THF (2.5 mL) and H<sub>2</sub>O (250 μL). The reaction vial was then placed into a 300 mL autoclave. The autoclave was flushed with hydrogen twice at 50 bar pressure, pressurized to 50 bar hydrogen pressure and placed into an aluminium block preheated at 110 °C. After the reaction was completed the autoclave was placed into a water bath and cooled to room temperature. Finally, the remaining hydrogen gas was discharged and the samples were removed from the autoclave. To the individual vials *n*-hexadecane as an internal standard was added, the crude product was diluted with ethyl acetate followed by filtration and analyzed by GC.

**Table S1.** Performance with different catalyst loadings.



Entry <sup>a</sup>	Catalyst loading [mol%]	Yield imine <b>1</b> <sup>b</sup>	Yield amine <b>2</b> <sup>b</sup>
<b>1</b>	0	—	—
<b>2</b>	1	32	42
<b>3</b>	2	16	79
<b>4</b>	3	10	84
<b>5</b>	4	9	85

<sup>a</sup> Reaction conditions: 0.5 mmol of nitrobenzene, 1.0 mmol of benzaldehyde, 3 ml solvent.

<sup>b</sup> Determined by GC using *n*-hexadecane as an internal standard.

## **S8. Catalyst recycling experiments**

For the catalyst recycling experiments, the reactions were carried out on a larger scale (2.5 mmol nitrobenzene, 5.0 mmol benzaldehyde). An autoclave (300 mL) was charged with a glass vial (20 mL) including the cobalt-catalyst (100 mg), nitrobenzene (295 μL) and benzaldehyde (444 μL) in a 10:1 THF/H<sub>2</sub>O-mixture (15 mL/1.5 mL). The autoclave was then flushed with hydrogen twice and charged with 50 bar of hydrogen. After each run the catalyst was isolated, washed with ethyl acetate and dried under vacuum overnight.

## **S9. References**

- [45] M. A. Mohamed, S. A. Halawy, M.M. Ebrahim, *J. Therm. Anal. Calorim.* **1994**, *41*, 387-414.
- [46] T. Wanjun, C. Donghua, *Chem. Pap.* **2007**, *61*, 329-332.
- [47] J. Casanovas, J.M. Ricart, J. Rubio, E. Illas, J.M. Jiménez-Mateos, *J. Am. Chem. Soc.* **1996**, *118*, 8071-8076.
- [48] J.R. Pels, F. Kapteijn, J.A. Moulijn, Q. Zhu, K.M. Thomas, *Carbon* **1995**, *33*, 1641-1653.
- [49] W. Grünert, R. Feldhaus, K. Anders, S.E. Shipiro, G. V. Antoshin, K.M. Minachev, *J. Electron. Spectrosc. Relat. Phenom.* **1986**, *40*, 187-192.
- [50] M.C. Biesinger, B.P. Payne, A.P. Grosvenor, L.W.M. Lau, A.R. Gerson, R.St.C. Smart, *Appl. Surf. Sci.* **2011**, *257*, 2717.
- [51] S. Angelov, E. Zhecheva, R. Stoyanova, M. Atanasov, *J. Phys. Chem. Solids* **1990**, *51*, 1157.
- [52] P. Dutta, M.S. Seehra, S. Thota, S. J. Kumar, *J. Phys.: Condens. Matter* **2008**, *20*, 15218.
- [53] A. Brückner, A. Martin, N. Steinfeldt, G.-U. Wolf, B.Lücke, *J. Chem. Soc. Faraday Trans.* **1996**, *92*, 4257-4263.
- [54] U. D. Wdowik, D. Legut, *J. Phys. Chem. Solids* **2008**, *69*, 1698-1703.
- [55] F.C. Campbel, *Elements of Metallurgy and Engineering Alloys*, **2008**, Materials Park, Ohio: ASM International, Chapter **29**, p. 557.